LBL-20163
c.2

Lawrence Berkeley Laboratory
UNIVERSITY OF CALIFORNIA

OCT 9

Invited talk presented at the Second International Conference on Nucleus-Nucleus Collisions, Visby, Sweden, June 10-14, 1985

UNRESOLVED GAMMA RAYS FROM HIGH-SPIN STATES

F.S. Stephens

August 1985

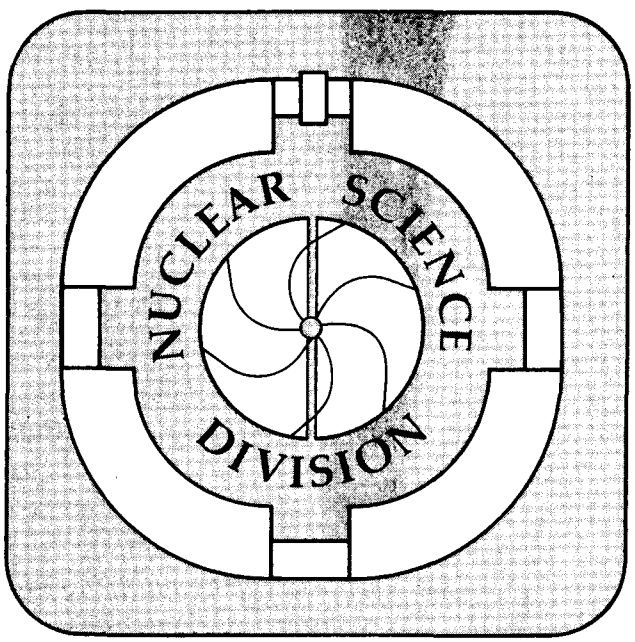

Prepared for the U.S. Department of Energy under Contract DE-AC03-76SF00098

LBL-20163
c.2

DISCLAIMER

This document was prepared as an account of work sponsored by the United States Government. While this document is believed to contain correct information, neither the United States Government nor any agency thereof, nor the Regents of the University of California, nor any of their employees, makes any warranty, express or implied, or assumes any legal responsibility for the accuracy, completeness, or usefulness of any information, apparatus, product, or process disclosed, or represents that its use would not infringe privately owned rights. Reference herein to any specific commercial product, process, or service by its trade name, trademark, manufacturer, or otherwise, does not necessarily constitute or imply its endorsement, recommendation, or favoring by the United States Government or any agency thereof, or the Regents of the University of California. The views and opinions of authors expressed herein do not necessarily state or reflect those of the United States Government or any agency thereof or the Regents of the University of California.

LBL-20163

Unresolved Gamma Rays from High-Spin States

F.S. Stephens

Nuclear Science Division
Lawrence Berkeley Laboratory
University of California
Berkeley, California 94720

Invited talk at the Second International Conference on Nucleus-Nucleus Collisions

Visby, Sweden 10-14 June, 1985

This work was supported in part by the Director, Office of Energy Research, Division of Nuclear Physics of the Office of High Energy and Nuclear Physics of the U.S. Department of Energy under Contract DE-AC03-76SF00098.

UNRESOLVED GAMMA RAYS FROM HIGH-SPIN STATES

F.S. Stephens, Nuclear Science Division, Lawrence Berkeley Laboratory, University of California, Berkeley, California 94720*

The γ rays emitted from the highest-spin states in nuclei cannot be resolved using present techniques. Nevertheless, methods are being developed to study nuclear structures in this spin range. While the general properties observed are in accord with present expectations, more detailed information seems to indicate some unexpected behavior.

1. INTRODUCTION

One view of nuclear physics at high spins is that it is just ordinary nuclear physics with the addition of Coriolis and centrifugal forces. It is fortunate both that we understand these forces very well and that we can make them large enough to perturb the nuclear structure in a major way. In fact, for medium and heavy nuclei, the limit on the amount of angular momentum the nucleus can hold comes when these forces literally pull it apart--causing fission.

Some appreciation of the energies involved comes from considering a nucleus of mass about 130 at a spin of about 70ħ--the maximum such a nucleus can hold. The rotational energy in such a case is around 35 MeV. The total pairing energy is an order of magnitude less--~3 MeV. Since generating angular momentum is basically inconsistent with the spin-zero coupling essential to the pairing, it is clear that the pairing will be quenched. How this happens is a fascinating story, but occurs at spins lower than I will be considering in this talk. The shell effects in nuclei are of order 10 MeV, and, again, will be dominated by the rotation. The nuclear shape, for example, is mainly determined by the shell structure at low spins but is increasingly modified by the rotational motion as the spins increase. The surface and Coulomb energies in such a nucleus are both about 500 MeV--considerably larger than the rotational energy. Nevertheless, these two major forces are balanced, and at 70ħ the centrifugal force becomes sufficient to tip the balance. An interesting step that sometimes occurs along the way to fission is the onset of very large deformations (called superdeformations), and that is one of two or three topics I will discuss.

It is reasonably easy to make nuclei with all the angular momentum they can

---

*This work was supported in part by the Director, Office of Energy Research, Division of Nuclear Physics of the Office of High Energy and Nuclear Physics of the U.S. Department of Energy under Contract DE-AC03-76SF00098.

hold using heavy-ion fusion reactions. A schematic illustration of the decay modes for a nucleus of mass ~160 is shown in the "phase-like diagram" of Fig. 1. The coordinates are nuclear excitation, E*, and spin, I. The heavy lines divide the E*-I space into regions of different decay modes. The yrast line is the locus of states of lowest energy for a given spin, so that no states exist in the nucleus below this line. A typical heavy-ion fusion reaction might lead to an initial excitation energy of ~65 MeV and a spin distribution ranging from 0 to ~65ħ as indicated by the light line in Fig. 1. As long as the nucleus has sufficient energy above the yrast line to emit nucleons (~10 MeV), it usually does so; γ-ray emission is too slow to compete well with particle evaporation. But at excitations below the nucleon binding energy, γ-ray emission takes over and de-excites the nucleus to its ground state. It is now known that these γ-ray cascades have two principal types of transitions. The "statistical" transitions carry off energy but little angular momentum and so cool the nucleus towards the yrast line (vertical in Fig. 1). The "yrast-like" transitions follow paths roughly parallel to the yrast line and remove the angular momentum of the system. These latter are sometimes collective rotational transitions, and sometimes not. There are an enormous number of pathways from the beginnings of a high-spin γ cascade until a region near the yrast line is reached, with the result that no single transition has enough intensity to stand up in the spectrum (with present techniques). This is the origin of the name "continuum" γ-ray spectrum, though this is not a true continuum. When the nucleus has cooled sufficiently the population condenses into a few pathways and the transitions in these pathways stand up in the spectrum and are resolved. This typically happens in the spin range 30-40ħ for masses around 160, and it provides a logical division in high-spin studies. In the lower-spin region, one can employ all the techniques of conventional γ-ray spectroscopy and develop detailed information on the nature of the transitions and states involved. John Sharpey-Schafer will discuss this region in the next lecture. At the higher spins where the population is spread out too much to permit the study of individual transitions, new techniques are providing a picture of the average nuclear behavior. This will be the subject of the present talk.

A typical γ-ray spectrum[1] following an ^{40}Ar fusion reaction is shown in Fig. 2. The statistical part, represented by the estimate, $E_\gamma^3 \exp(-E_\gamma/T)$, is shown as a dashed line. While not so accurately known, this part of the spectrum is small below ~2 MeV. There are resolved lines below 1-1.5 MeV, which are not seen well in this low-resolution (NaI) spectrum. The unresolved yrast transitions form the bump extending up to ~2.5 MeV. In some respects

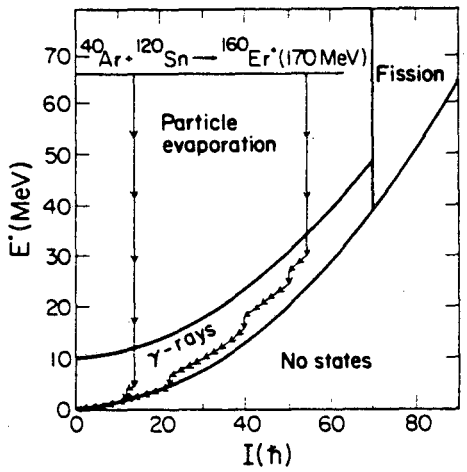

FIGURE 1
The heavy lines constitute a phase-like diagram for the decay modes of a nucleus having mass number about 160 as a function of excitation energy and angular momentum. The lighter horizontal line indicates the range of angular momentum brought in by a typical heavy-ion reaction, following which two of the many possible decay pathways are shown (longer arrows represent neutron evaporations and shorter ones γ-ray emissions).

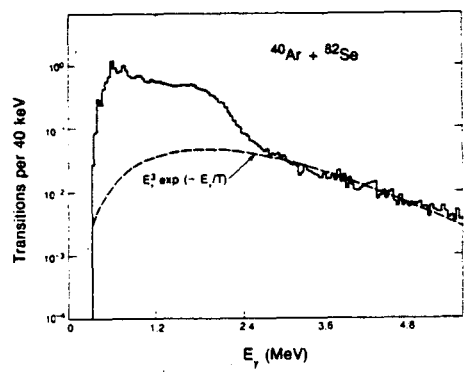

FIGURE 2
Gamma-ray spectrum observed for the ^{40}Ar + ^{82}Se reaction. The statistical component of the spectrum that is subtracted to obtain the "yrast-like" transitions is shown as a dashed line. For this case the temperature T was 0.6 MeV.

it is unfortunate that they occur at higher temperatures and cannot be resolved. On the other hand this gives us the opportunity to study the effects of temperature on rotation--another topic that I will discuss.

2. MOMENTS OF INERTIA

We are able to interpret unresolved spectra mainly through studying moments of inertia. There has been some conflicting nomenclature in this area, but the subject is rather simple, except for a couple of small problems. The first problem is that the moments of inertia are not constant. There are several ways this might be handled, but the way usually chosen is to define an average moment of inertia (from spin zero to I) defined as $\mathcal{J}^{(1)}/\hbar^2 = I/\omega$, and a differential or local value, $\mathcal{J}^{(2)}/\hbar^2 = dI/d\omega$. Both the spin, I, and the rotational frequency, ω, are experimentally accessible, since $\omega \sim E_\gamma/2$, where E_γ is the rotational transition energy. The second problem is that there are really are two kinds of angular momentum. This point is illustrated in Fig. 3, where the lowest high-spin levels of ^{158}Er contrast strongly with those of the nearby nucleus ^{147}Gd. In ^{158}Er the angular momentum arises mostly from a collective rotation, while for ^{147}Gd it is from the alignment

of individual nucleons. At high spins, these two modes of generating angular momentum both contribute and can be at least partly distinguished. We have $I = I_{coll} + i$, where I_{coll} is the rotational part, and i is the aligned (non-collective) part. Two independent types of moment of inertia can thus be defined, and the experimental measurables suggest that these be: (1) "effective" moments of inertia ($\mathcal{J}^{(1)}_{eff}$ and $\mathcal{J}^{(2)}_{eff}$) based on the <u>total</u> angular momentum, I, irrespective of whether it really comes from collective rotation or not; and (2) "collective" or "band" values based on I_{coll}. The $\mathcal{J}^{(1)}_{coll}$ values are not really accessible, since they would require separating a particular I into its components, I_{coll} and i--not usually possible. However, the $\mathcal{J}^{(2)}_{coll}$ are accessible since one can usually determine whether a given transition (ΔI) is a collective one or not. Thus our knowledge of the unresolved γ-rays comes mostly from three types of moments of inertia.

3. EFFECTIVE MOMENTS OF INERTIA

Many of the general properties of the high-spin states can be deduced by studying the effective moments of inertia. Three spectra[1] from the reaction $^{40}Ar + {}^{82}Se$ (175 MeV) are shown in Fig. 4. These are due mostly to ^{118}Te (the 4α product) and resolved ^{118}Te lines are seen below about 1.5 MeV. The three spectra come from coincidences with the three indicated regions of a total γ-ray energy spectrum, obtained from a large NaI crystal that surrounded the ^{82}Se target. Higher total energies correspond to higher average spins, and the effect on the yrast-like transitions in Fig. 4 is clear--they increase in energy. The reason is thought to be that they are rotational-type γ-rays, and have the rotational dependence on spin: $E_\gamma \propto I$. In fact, in virtually all cases so far studied the yrast-like transitions from the highest spin states are thought to be basically rotational. This is because: (1) they are always predominantly stretched E2 type ($I \rightarrow I-2$); (2) they have energies correlated with spin (as for ^{118}Te in Fig. 4); and (3) in at least a few cases their lifetimes have been measured and they are fast--indicating collective enhancements of order 100 times the single-particle value. Thus there is very likely rotational-type behavior at the highest spins.

If the behavior is basically rotational then it is easy to see that the height of the spectrum is directly related to $\mathcal{J}^{(2)}_{eff}$. The height is the number of γ-rays per γ-ray energy interval, and while the number of γ-rays is just half the change in spin (for stretched E2 transitions), the γ-ray energy interval is twice the frequency interval. Thus the spectrum height is $\mathcal{J}^{(2)}_{eff}/4\hbar^2$. There are corrections having to do with the amount of population at each energy, but that will not be discussed here. The spectra may be

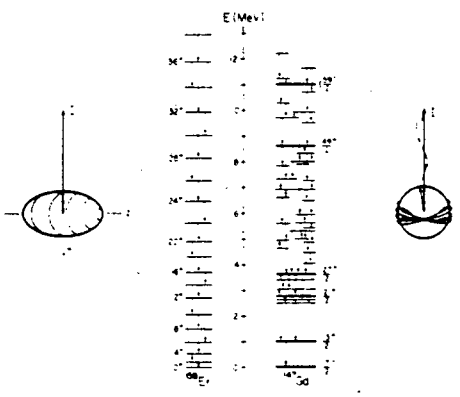

FIGURE 3
The level schemes are for the lowest-energy high-spin states in ^{158}Er and ^{147}Gd[2,3]. The sketches on the left and right sides of the figure illustrate the dominant source of angular momentum in each case, collective rotation and single-particle alignment, respectively.

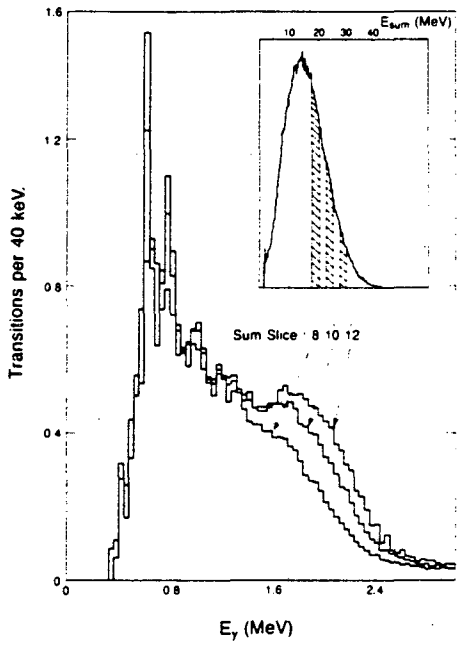

FIGURE 4
Normalized unfolded spectra for the reaction ^{40}Ar + ^{82}Se in coincidence with different sum slices as shown in the insert. The sum slices are 2.5 MeV wide and are numbered starting from 0 MeV.

integrated to give $\mathcal{J}^{(1)}_{eff}$ and the values for several systems are compared with those for a rigid sphere in Fig. 5. These $\mathcal{J}^{(1)}_{eff}$ values are not for a specific product, but that is not likely to be important since such gross properties are expected to be smooth over limited mass regions. The $\mathcal{J}^{(1)}_{eff}$ values are rather structureless and close to the rigid-sphere value, as is expected from estimates[5] based on an anisotropic harmonic oscillator.

The values of $\mathcal{J}^{(2)}_{eff}$ shown in Fig. 6 have somewhat more structure. They are plotted against a normalized frequency as will be discussed. These $\mathcal{J}^{(2)}_{eff}$ values seem to oscillate between 1 and 1.5 times the rigid-sphere value, and whereas most of them are reasonably similar, the values for the ^{130}Te target are not. The probable explanation for this behavior is illustrated in Fig. 7. For a certain range of frequencies (or spins) the angular momentum will be generated out of nucleons in the valence shell. These are expected to give moments of inertia around the rigid-sphere value. But at some frequency the the high-j orbitals from the next major shell will reach the region of the

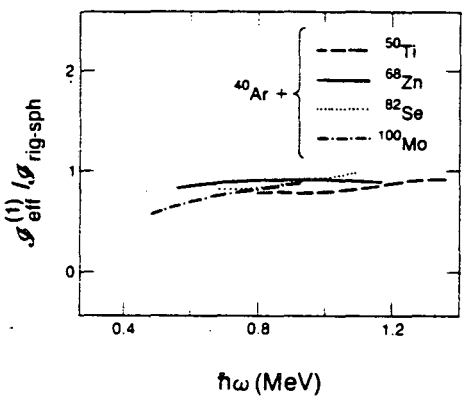

FIGURE 5
Some results for $\mathcal{J}^{(1)}_{eff}$ in units of the rigid-sphere value $\frac{\mathcal{J}_{rig-sph}}{\hbar^2}$ = 0.0139 $A^{5/3}$ MeV^{-1}. The four indicated targets were bombarded with ^{90}Ar projectiles, resulting in several product nuclei in each case.

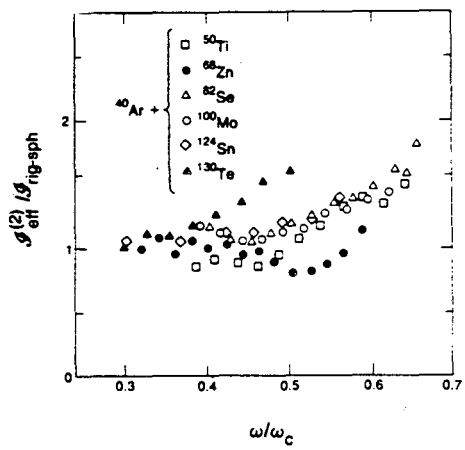

FIGURE 6
Some $\mathcal{J}^{(2)}_{eff}$ values in units of $\mathcal{J}_{rig-sph}$ as a function of the reduced frequency (ω/ω_c). Two target nuclei, in addition to those of Fig. 5, are shown.

Fermi level, and contribute additional angular momentum--increasing $\mathcal{J}^{(2)}_{eff}$. The exact frequency value where this occurs will depend on the deformation and the position of the Fermi level, but the right portion of Fig. 7 shows that the highest-j values have a slope around $A^{1/3}$, and thus cover the distance between major shells in a frequency interval around $41/A^{2/3}$. This is the scale parameter, ω_c, of Fig. 6, and gives the maximum frequency for effects due to the next major shell. It is seen that the increases in $\mathcal{J}^{(2)}_{eff}$ come at frequencies comparable with, but smaller than, this ω_c.

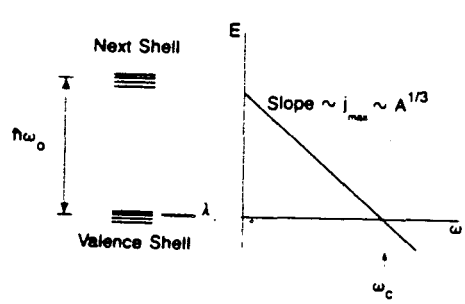

FIGURE 7
Simplified shell model, illustrating how a high-j orbital from the next shell approaches the Fermi surface, λ (valence shell), under the influence of rotation. As discussed in the text, ω_c follows an $A^{-2/3}$ dependence.

Some details of the ^{40}Ar + ^{130}Te system of Fig. 6 are shown in Fig. 8.

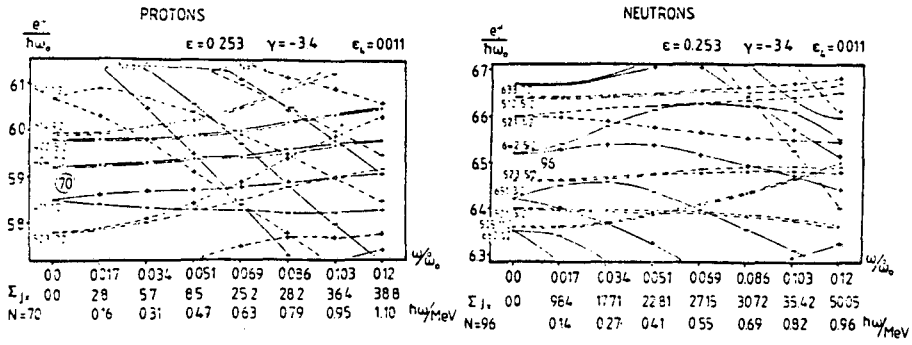

FIGURE 8
Calculated level diagrams[6] for protons (left) and neutrons (right) in ^{166}Yb. The ordinate is energy (in units of the shell-model oscillator energy) and the three abcissa scales are: top, rotational frequency (in units of the shell-model oscillator frequency); middle, the total spin generated; and bottom, the rotational frequency in MeV/ħ.

These are portions of the calculated level diagrams[6] (energy vs. frequency) for protons and neutrons in ^{166}Yb, the main product of that system. The Fermi levels at 70 protons and 96 neutrons are indicated. The levels from the valence shell are more or less horizontal, indicating that they can contribute little or no additional angular momentum. However, the lowest-energy high-j levels from the next major shells are coming down steeply on both plots (541-1/2 and N = 6 for protons; and those that cut off the upper right corner for neutrons). They have large angular momenta to contribute (proportional to the slope) when they reach the Fermi level and become occupied. It can be seen that this happens around frequencies of 0.5 for protons and 0.8 for neutrons. Thus the early rise for the ^{130}Te system on Fig. 6 at $\omega/\omega_c \sim 0.4$ ($\omega \sim 0.5$) is very likely due to contributions from the next higher proton shell. Similar detailed analysis can be made for the other cases, and generally work well. The present conclusion from studying the effective moments of inertia is that we understand rather well the gross features of angular momentum generation. The detailed behavior, however, is still largely a mystery as we shall see.

4. E_γ-E_γ CORRELATIONS

The collective moment of inertia $\mathcal{J}^{(2)}_{coll}$ can also be measured, at least approximately. A typical rotational band is shown on the left side of Fig. 9. The level energies are proportional to I(I + 1) so that the transition energies (shown on the right) are proportional to I--equally spaced. If coincidence data are plotted as $E_\gamma(1)$ against $E_\gamma(2)$, plots like those in

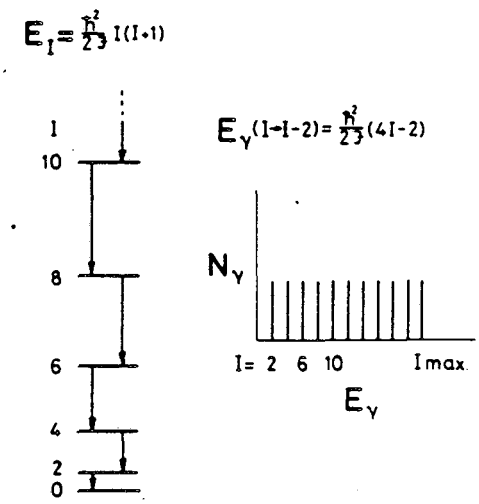

FIGURE 9
An idealized rotational band (left) and the resulting γ-ray spectrum from an initial state of spin, I_{max} (right).

Fig. 10 result. On the left, coincidences from four cascades are plotted, where they all have the same $\mathcal{J}^{(2)}_{coll}$, but different alignments, i. The resulting pattern has nothing along the diagonal (no two γ-rays have the same energy), and then a series of ridges parallel to the diagonal. The width of the valley along the diagonal is related to $\mathcal{J}^{(2)}_{coll}$. On the right side of Fig. 10 a more realistic case is shown. There are variations in $\mathcal{J}^{(2)}_{coll}$, and also some irregularities that cause events in the valley. There is a large amount of data that looks rather similar to the right side of Fig. 10. I will not review these data here, but only give you one example--perhaps the most striking.

One of the experimental objectives for high-spin studies over a number of years has been to identify superdeformed nuclei. These elongated shapes (axis ratio, 2:1) should occur somewhat prior to high-spin fission in much the same way as the (superdeformed) fission isomers in the actinide region occur just prior to the onset of low-spin fission. Perhaps the best evidence to date for high-spin superdeformation is shown[8] in Fig. 11. This is an E_γ vs. E_γ correlation plot for ^{152}Dy, which is not a rotational nucleus at low spins. A background of uncorrelated events has been subtracted from Fig. 11. The vertical and horizontal lines are due to strong resolved lines, which are not important here. There is also, however, a distinct valley and ridges that run from ~0.8 to ~1.3 MeV. This indicates a rotational behavior, and the width of the valley corresponds to $\mathcal{J}^{(2)}_{coll} \approx 85$ MeV^{-1}. Since this is appreciably above the value expected for normal deformation (~70 MeV^{-1}) it is taken as

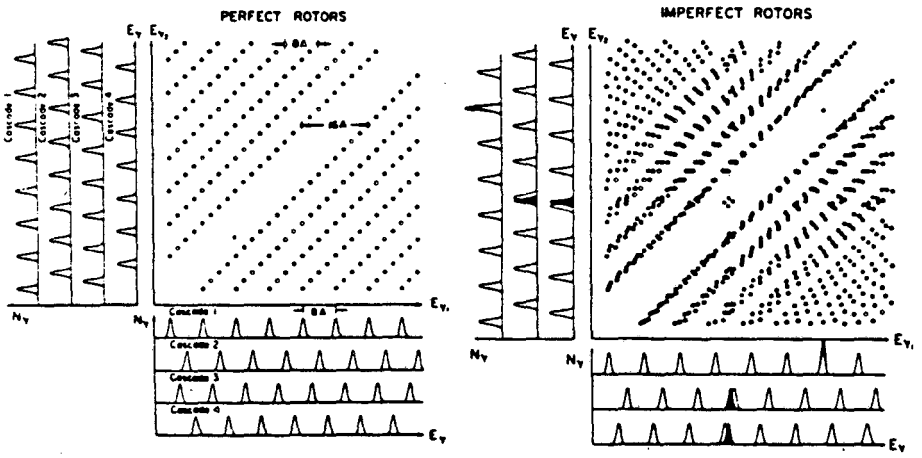

FIGURE 10
Schematic $E_{\gamma 1}$ vs. $E_{\gamma 2}$ correlation plots for: left, four bands having the same $\mathcal{J}^{(2)}_{coll}$, but different i values; right, same four bands plus four more with 10% larger $\mathcal{J}^{(2)}_{coll}$ and four with 10% smaller $\mathcal{J}^{(2)}_{coll}$, and some irregularities--solid peaks and points[7].

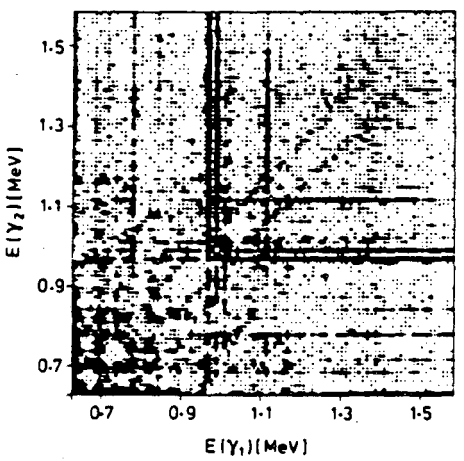

FIGURE 11
A plot showing the $E(_{\gamma 1})$-$E(_{\gamma 2})$ correlations in ^{152}Dy following the reaction of 205 MeV ^{48}Ca on ^{108}Pd. The The data were taken with Compton-suppressed Ge detectors, have been corrected for the response function and efficiency of the detectors, and have had uncorrelated events subtracted by an iterative procedure[8].

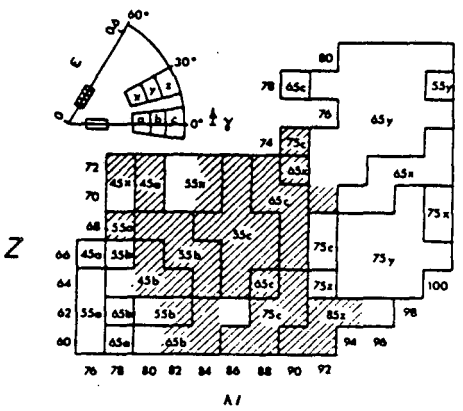

FIGURE 12
Calculated high-spin equilibrium shapes for nuclei in a region of Z and N. The letters refer to shapes indicated on the Eus γ plot at upper left. The numbers are the spins at which that shape is calculated to become stable.

evidence for larger (super) deformation.

Nuclear properties such as deformation are rather reliably calculated now. Figure 12 shows a chart of Z vs. N, on which is indicated the stable high-spin

shape, and the spin at which it becomes lowest in energy[9]. The traditional "superdeformed" shape corresponds to the letter "c" and one sees that for $_{86}Dy^{152}_{66}$ the spin at which this shape becomes stable is the lowest in the entire region -55ħ. Rough estimates for the valley and ridges in Fig. 11 would be about 35-60ħ--in reasonable accord with the calculations. Thus experiment and calculation are in reasonable agreement that there is superdeformation in ^{152}Dy. One also sees that the E_γ-E_γ correlation plots represent a powerful way to estimate $\mathcal{J}^{(2)}_{coll}$, and thereby nuclear properties like deformations.

5. CORRELATION PROPERTIES OF UNRESOLVED GAMMA RAYS

There are, however, some major puzzles apparent in the correlation plots. In general above about 1 MeV, the ridges disappear and at about that point the valley gets shallow and eventually it too disappears. Absent or weak ridges indicate deviations from simple rotational motion, and this will tend (more slowly) to fill the valley as well. In order to determine the nature of these deviations, the most reliable quantities to measure are the width and the depth of the valley. The measured width depends *a priori* on the moment of inertia and the detector resolution. Theses are comparable for NaI detectors (about 60 keV at 1 MeV γ-ray energy) which were used in the first experimental determinations. However, the lack of a strong valley in high-resolution spectra (Ge detectors) implies, in addition, an irregularity or spread in the γ-ray energies *within a given decay pathway* (i.e. not just a spread in moments of inertia for different pathways). We call this the γ-ray spread, and it both fills in and broadens the valley. Above $E_\gamma \sim 1$ MeV this spread produces a valley that is wide enough to be measurable with NaI resolution. Over the last two years techniques have been developed[10] to measure independently the width and the depth of this valley. Using a simple model one can then determine the γ-ray spread from the measured valley width.

To measure the valley width, the general idea was to vary a gate width, W, and look for a change in the coincident dip when these two widths become comparable. The analysis involves the coincident spectra for pairs of contiguous gates of various widths 20-200 keV and of median energies 720, 840, 960, 1080 and 1200 keV. For such a pair, illustrated in Fig. 13a, d_2 is normalized to d_1, and the spectra are subtracted as in Fig. 13b. The variation (not the magnitude) of the height, H, vs. W is first analyzed. This gives the σ_γ of the assumed Gaussian γ-ray spread. Then the ratio H/d is analyzed to give, almost independently, the filling in of the valley due to other wider components of the spreading. Fig. 14 shows the data for 100 keV

gates with a common boundary at 840 keV. The top spectrum is for the higher gate; the bottom shows both the experimental and calculated difference spectra. The quantity most reliably obtainable from the data is the H shown

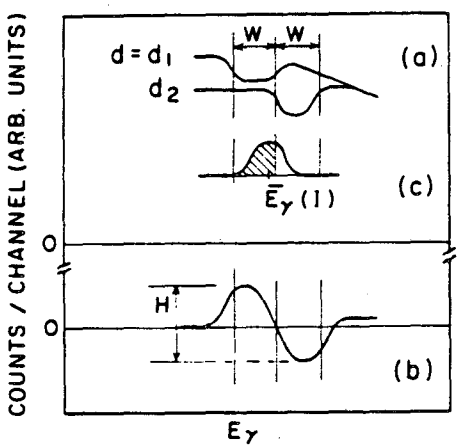

FIGURE 13
(a) Portions of coincidence spectra (schematic) for lower and upper contiguous gates of widths W.
(b) Difference of spectra in (a) after normalizing d_2 to $d_1 \equiv d$.

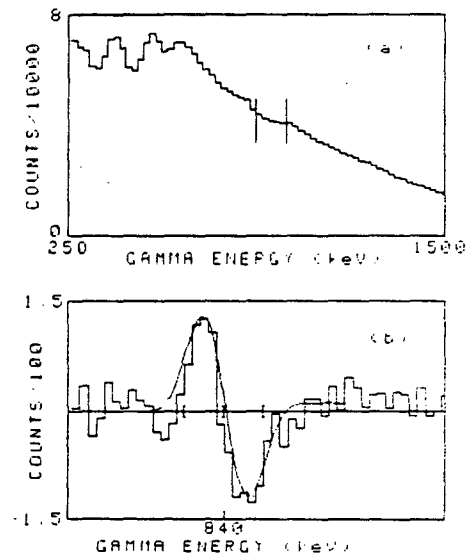

FIGURE 14
(a) Coincidence spectrum for 840-940 keV gate (vertical lines).
(b) Difference spectrum for gates 840-940 and 740-840 keV, indicated, using spectrum (a). The smooth curve is calculated and uses the width deduced from Fig. 3. Experimental spectra in (a) and (b) are raw data at 20 keV/channel.

in Fig. 13b. In Fig. 15 is plotted H/W vs. W/σ_{tot} for the best choice of σ_{tot}, which is found through iteration. The σ_{tot} value contains also the effects of the NaI detector resolution, which can be removed to give σ_γ. The experimental results represented in Fig. 15 show that there is a dominant γ-ray spread causing the observed valley. The FWHM from this varies from <40 keV at 720 keV γ-ray energy to 125 ± 20 keV at 1200 keV γ-ray energy. However, 80-90% of the population does not contribute to this valley, as indicated by its very small depth. Presumably this larger part of the population has considerably wider correlations; however, these first measurements really only give information about the 10-20% that cause the observed valley.

The significance of the measured γ-ray spread has become much clearer recently. The high-spin γ-ray spectra are thought to be unresolved because

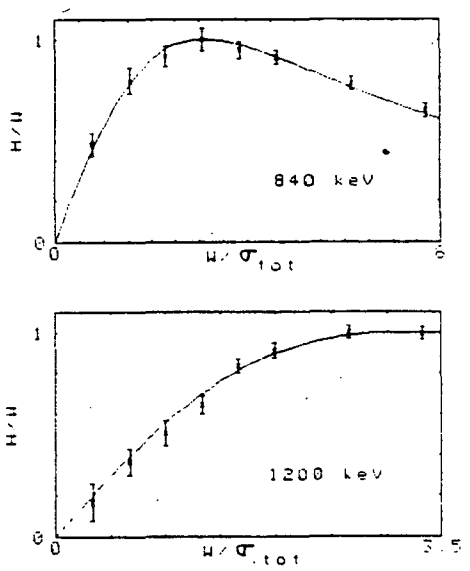

FIGURE 15
Examples of fits of calculations to the experimental points to determine σ_{tot} for gates with the common energy shown. The maxima of both curves are normalized to unity. After iterations on σ_{tot}, the final fits are shown in this figure.

they occur before the population "cools" to the yrast line--i.e. they occur at non-zero temperatures where the density of background states is high. Some implications of this were considered by Leander[11], and recently developed by Døssing et al.[12]. It is well know that a given shell-model state in a region of high level density will be mixed (by residual interactions) into the other states over a region called the damping (or spreading) width, which increases with level density. If there were no changes in the internal nuclear structure as a function of spin, such a spreading would *not* lead to a γ-ray spread for rotational nuclei. However, there *are* changes in the internal structure--the leading order (expected) effects being due to the Coriolis interaction which tends to produce rotationally aligned particle motion that is quantized in the sense that a given state will contain certain aligned particles, but not others. For a given spin this gives rise to a spread in particle alignments or, in other words, a distribution of moments of inertia. In the absence of a damping width this distribution of moments of inertia would produce a superposition of sharp ridges, which would broaden the ridge, but never fill the valley inside a limit given by the largest moment of inertia--nothing like the experimental observation. However, as soon as a given level has damped so that it has components with the different moments of inertia, it no longer emits a single γ-ray energy (characterized by its

moment of inertia), but can emit a distribution of γ-ray energies corresponding to the admixed distribution of moments of inertia. This is the situation represented in the experiment analysis, and one that can reproduce the experimental observations. Thus it is plausible that the measured γ-ray spreads result from the damping of rotational bands. It should be emphasized, however, that this subject is still quite young, and the γ-ray spreads could be due to other processes. In addition, the relationship of the bulk of the population (80-90%) to the 10 to 20% producing these spreads is not at all clear. It will be quite interesting to characterize better both the unresolved γ-ray properties and the origin of such properties.

6. HIGHER-ORDER CORRELATIONS

The new γ-ray detector systems--of up to ~20 Compton-suppressed germanium detectors--are making some new types of measurement possible. One of these is the study of correlations among more than two γ-rays. A reasonably straightforward example[13] of this is shown in Fig. 16, which is an E_γ-E_γ correlation

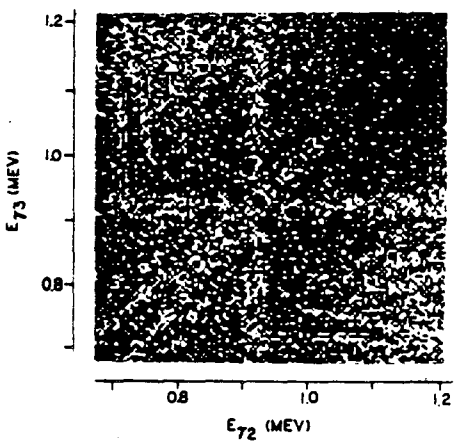

FIGURE 16
An $E_{\gamma 2}$-$E_{\gamma 3}$ correlation plot, where $E_{\gamma 1}$ has been set at 0.920 ± 0.012 MeV. A background of uncorrelated events has been subtracted.

matrix in coincidence with a third γ-ray--$E_{\gamma 1}$ = 0.920 ± 0.012 MeV. The rotational correlation condition that no two γ-rays have the same energy, produces three valleys on this plot. The usual valley along the diagonal results because $E_{\gamma 2}$ and $E_{\gamma 3}$ tend not to have the same energy. But there are also vertical and horizontal valleys that occur because $E_{\gamma 2}$ and $E_{\gamma 3}$ tend not to have the same energy as $E_{\gamma 1}$. The interesting point is the intersection of the three valleys, where all three γ-rays have the same energy. There is a hole there that is deeper than the adjacent valleys. The analysis of this

behavior has barely begun, but it says immediately that three γ-rays of the same energy are significantly less probable than two of the same energy. For this to be true requires that in those sequences producing the valleys there are often three successive γ-ray transitions in the same rotational band. This seems to conflict with recent measurements[14] that show that the probability to branch out of a rotational sequence is high. However, when taken together with the results of the previous section, which show that these valleys are caused by only ~10% of all cascades, there is probably no experimental contradiction--only evidence that we are dealing with several separate kinds of cascades, none of which is understood very well yet. There is now a large effort to understand quantitatively spectra like those in Fig. 16.

The promise of the higher-order correlations is illustrated by the above discussion. The correlated properties of the events one wants to study are used to generate a "filter" for those events. In the above example, the rotational property that no two γ-rays have the same energy is being used to study rotational behavior through the study of the resulting valleys in E_γ-E_γ correlation plots. This particular plotting technique is a filter for such behavior. Other more complicated filters can be constructed to study other types of behavior.

A related, but more complex, example is the search for superdeformations now being conducted using quadrupole coincidences events. Use is made of the expectation that superdeformed nuclei will have large moments of inertia, which result in rotational transitions whose energies differ by about 40 ± 10 keV in the rare-earth region. Thus to filter out such cases one orders the four γ-ray energies and requires that the $E_{\gamma 2}-E_{\gamma 1}$ = 40 ± 10 keV and also that $E_{\gamma 4}-E_{\gamma 3}$ = 40 ± 10 keV. In typical cases this should retain all superdeformed cascades of four successive transitions, while reducing other types by a factor of ~10^3. A plot of the average energy of $E_{\gamma 1}$ and $E_{\gamma 2}$ vs. that of $E_{\gamma 3}$ and $E_{\gamma 4}$ results in a correlation plot similar to that of Fig. 11, where the presence of superdeformed cascades is revealed by ridges ~80 keV on either side of the diagonal, whereas the absence of such cascades gives only a random distribution of points on the plot. The advantage is the enrichment of ~10^3 in the superdeformed events. Two nuclei ^{166}Yb and ^{160}Er have been so far studied[15] in this way, and no evidence for superdeformations was seen (or expected in these cases). Study of ^{152}Dy by this technique is now underway--the case discussed in connection with Fig. 11. The important point here is to illustrate that higher-order coincidences offer a very general way to filter out events of interest and study them. I believe it represents a significant advance in the experimental techniques to study high-spin states, as well as many other phenomena.

ACKNOWLEDGMENTS

This work was supported by the Director, Office of Energy Research, Division of Nuclear Physics of the Office of High Energy and Nuclear Physics of the U.S. Department of Energy under Contract DE-AC03-76SF00098.

REFERENCES

1) A.O. Macchiavelli et al., Nucl. Phys. A443 (1985) 538.

2) J. Burde et al., Phys. Rev. Lett. 48 (1982) 530.

3) P. Kleinheinz et al., Z. Phys. A290 (1979) 279.

4) M.A. Deleplanque et al., submitted to Nuclear Physics.

5) A. Bohr and B.R. Mottelson, Phys. Lett. 115B (1982) 431.

6) T. Bengtsson and I. Ragnarsson, Phys. Lett. 115B (1982) 431.

7) B. Herskind, Jour. de Phys. C10 (1980) 106.

8) B.M. Nyako et al., Phys. Rev. Lett. 52 (1984) 507.

9) S. Åberg, Phys. Ser. 25 (1982) 23.

10) J.E. Draper et al., submitted to Phys. Rev. Lett.

11) G. Leander, Phys. Rev. C25 (1982) 2780.

12) T. Døssing, Niels Bohr Centennial Symposium on Nuclear Structure, Copenhagen, May, 1985, in press.

13) B. Herskind et al., unpublished data, 1985.

14) D.J.G. Love et al., Phys. Rev. Lett. 54 (1985) 1361.

15) M.A. Deleplanque et al., unpublished data.

This report was done with support from the Department of Energy. Any conclusions or opinions expressed in this report represent solely those of the author(s) and not necessarily those of The Regents of the University of California, the Lawrence Berkeley Laboratory or the Department of Energy.

Reference to a company or product name does not imply approval or recommendation of the product by the University of California or the U.S. Department of Energy to the exclusion of others that may be suitable.

LAWRENCE BERKELEY LABORATORY
TECHNICAL INFORMATION DEPARTMENT
UNIVERSITY OF CALIFORNIA
BERKELEY, CALIFORNIA 94720